PHYSICAL REVIEW C VOLUME 57, NUMBER 2 FEBRUARY 1998

Particle production at high baryon density in central Au+Au reactions at 11.6*A* GeV/*c*

L. Ahle,[8] Y. Akiba,[5] K. Ashktorab,[1] M. D. Baker,[8] D. Beavis,[1] H. C. Britt,[7] J. Chang,[3] C. Chasman,[1] Z. Chen,[1] C.-Y. Chi,[4] Y. Y. Chu,[1] V. Cianciolo,[7,8] B. A. Cole,[4] H. J. Crawford,[2] J. B. Cumming,[1] R. Debbe,[1] J. C. Dunlop,[8] W. Eldredge,[3] J. Engelage,[2] S.-Y. Fung,[3] J. J. Gaardhoje,[9] E. Garcia,[13] M. Gonin,[1] S. Gushue,[1] H. Hamagaki,[5] A. Hansen,[9] L. Hansen,[9] R. S. Hayano,[10] G. Heintzelman,[8] S. Homma,[5] E. Judd,[2] H. Kaneko,[6] J. Kang,[12] E.-J. Kim,[12] A. Kumagai,[11] K. Kurita,[11] J.-H. Lee,[1] M. J. Levine,[1] J. Luke,[7] Y. Miake,[11] A. Mignerey,[13] D. Morrison,[8] B. Moskowitz,[1] M. Moulson,[4] C. Muentz,[1] S. Nagamiya,[4] M. N. Namboodiri,[7] C. A. Ogilvie,[8] J. Olness,[1] S. Park,[8] L. P. Remsberg,[1] P. Rothschild,[8] H. Sako,[5] T. C. Sangster,[7] R. Seto,[3] J. Shea,[13] K. Shigaki,[10] R. Soltz,[7,8] S. G. Steadman,[8] G. S. F. Stephans,[8] T. Sung,[8] M. J. Tannenbaum,[1] J. H. Thomas,[7] S. Tonse,[7] S. Ueno-Hayashi,[11] F. Videbæk,[1] F. Wang,[4] Y. Wang,[4] Y. Wu,[4] H. Xiang,[3] G. H. Xu,[3] K. Yagi,[11] D. Zachary,[8] W. A. Zajc,[4] F. Zhu,[1] and Q. Zhu[3]

(E-802 Collaboration)

[1]*Brookhaven National Laboratory, Upton, New York 11973*
[2]*University of California, Space Sciences Laboratory, Berkeley, California 94720*
[3]*University of California, Riverside, California 92507*
[4]*Columbia University, New York, New York 10027*
and Nevis Laboratories, Irvington, New York 10533
[5]*Institute for Nuclear Study, University of Tokyo, Tokyo 188, Japan*
[6]*Kyoto University, Sakyo-ku, Kyoto 606, Japan*
[7]*Lawrence Livermore National Laboratory, Livermore, California 94550*
[8]*Massachusetts Institute of Technology, Cambridge, Massachusetts 02139*
[9]*Niels Bohr Institute for Astronomy, Physics, and Geophysics, University of Copenhagen, Denmark*
[10]*Department of Physics, University of Tokyo, Tokyo 113, Japan*
[11]*University of Tsukuba, Tsukuba, Ibaraki 305, Japan*
[12]*Yonsei University, Seoul 120-749, Korea*
[13]*University of Maryland, College Park, Maryland 20742*

(Received 13 June 1997)

Semi-inclusive proton and pion distributions from central Au+Au reactions at 11.6*A* GeV/*c* have been measured. The proton rapidity distribution shows significantly increased stopping compared to lighter systems, providing strong evidence for the formation of a state of matter with baryon density substantially greater than normal nuclear matter. Unlike reactions at this energy induced by lighter heavy ions, at low m_t-m_0 the proton invariant spectra deviate from a single exponential shape and become flatter, while π^- spectra are found to rise faster than the π^+ spectra. [S0556-2813(98)50402-5]

PACS number(s): 25.75.−q, 13.85.Ni, 21.65.+f

Interest in collisions between heavy ions at energies about 10*A* GeV stems from the large amount of energy deposited in the reactions. Some of the phenomena which have been considered to be associated with this energy loss include effects of the compression and heating of nuclear matter, the production of a state of very high baryon density, and the achievement of thermal and chemical equilibrium. Most speculatively, it has been conjectured that a sufficiently high baryonic density can be attained to effect a phase change from the initial hadronic matter to a quark-gluon plasma. The basic information about the dynamics of these reactions comes from measurements of the transverse momentum and rapidity distributions of hadron spectra. In particular, the proton distributions allow the determination of the kinetic energy dissipated in the reactions. Hadron spectra which result from collisions of silicon beams at 14.6*A* GeV/*c* with targets ranging from aluminum to gold have been studied extensively [1,2]. These studies indicate that the projectiles deposit essentially all their energy in targets larger than copper [3]. It is anticipated that with Au targets and Au projectiles at incident energy of 10*A*–15*A* GeV an interaction region of larger volume, higher maximum density, and longer lifetime can be achieved, offering an exciting new opportunity to study properties of nuclear matter far from its normal state. With the installation of the booster, the Brookhaven Tandem-AGS complex is capable of accelerating Au ions with momentum up to 11.6*A* GeV/*c*. In this paper we report the first proton and pion transverse momentum spectra and rapidity distributions for the important mid-rapidity region in Au+Au reactions. Comparisons with reactions induced by lighter ions at this energy are also discussed.

The E-866 experimental apparatus consists of two parts: event-characterizing global detectors to determine the centrality of the collision, and two magnetic spectrometers to track and identify the produced particles in different kinematic regions. In this paper, data are presented for events selected by software cuts requiring a small energy deposition in the zero degree calorimeter, corresponding to the most central 350 mb of cross section. The interaction trigger is formed by a valid beam particle with a charge loss of greater than 5 after traversing the 975 mg/cm^2 Au target. The details of the calorimeter are described elsewhere [2,4]. One of the

magnetic spectrometers, the larger aperture spectrometer, has also been described in detail elsewhere [1,2,4,5]. Particle identification by time-of-flight is achieved up to 1.8 GeV/c for pions, and 3.4 GeV/c for protons. Because of the high particle density produced in Au+Au reactions, this spectrometer is used to measure particles with emission angles larger than 24 degrees in the laboratory.

Smaller angles are covered by the newly implemented forward spectrometer which measures from 6 to 28 degrees. The forward spectrometer, with an aperture of about 5 msr, consists of two magnets, two tracking stations, and a time-of-flight wall. The first magnet is usually operated at 2 kG, and its purpose is to sweep away low momentum particles, including delta rays, in order to reduce the hit multiplicity on the first tracking station which follows this magnet. The second magnet, placed between the two tracking stations and operated at 4 or 6 kG, is used to analyze particle momentum. Each tracking station consists of a time-projection chamber sandwiched between a pair of projective drift chambers. The three-dimensional tracking information from the time-projection chambers provides excellent pattern recognition for particle trajectories, while the better spatial resolution of the drift chambers provides an accurate position determination for the final track. Particle identification for the forward spectrometer is obtained by measuring particle flight time to a 100-slat array of plastic scintillators located behind the second tracking station, about 6 meters away from the target. A timing resolution of 75 ps (1σ) is obtained. Particle identification is achieved up to 4 GeV/c for $\pi^{\pm}$, 5 GeV/c for protons. A momentum cut of 0.5 GeV/c is applied to exclude low momentum tracks from the analysis. Electrons and positrons are separated from pions with 5σ at 0.7 GeV/c, and 3 σ at 1 GeV/c.

For the forward spectrometer, track reconstruction starts at each tracking station independently, and straight trajectories are constructed at this stage. The straight lines from the two tracking stations are joined inside the analyzing magnet by taking an effective edge approximation, and the momentum associated with the trajectory is then calculated. The trajectory is projected toward the target through the first magnet with the calculated momentum by the method of ray tracing. Runs of zero magnetic field taken at each spectrometer angle serve to calibrate the tracking chambers precisely. The track-reconstruction efficiency was studied by visual reconstruction of 200 events at both the 6 degree and the 14 degree settings to identify the mechanism for track loss, and the correction factors are obtained by sorting the data for time-projection-chamber row distributions and time-of-flight wall hit distributions. The main cause of lost tracks is due to the higher slat occupancy of the time-of-flight wall (TOF) at forward angles from the background, resulting in an average correction factor of about 15% for the worst case.

Figure 1 shows the measured invariant spectra for protons at different rapidity intervals. On the horizontal axis, m_t is the ''transverse mass'' defined as $m_t=\sqrt{p_t^2+m_0^2}$, where p_t is the transverse momentum and m_0 is the rest mass of the identified particle. On the vertical scale is the invariant cross section divided by the trigger cross section σ_{trig} where σ_{trig} $=350$ mb. The solid points are the measurements from the forward spectrometer (taken in 1994) while the open ones are from the large aperture spectrometer (taken in 1992). The

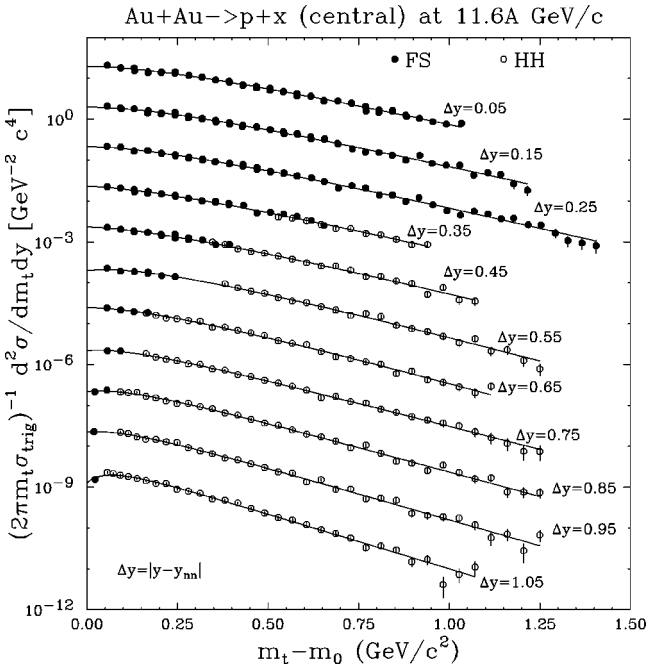

FIG. 1. Measured invariant cross section divided by the trigger cross section for identified protons in different rapidity intervals as a function of transverse kinetic energy m_t-m_0 (see text). The bin width of the rapidity interval is 0.1, and Δy is the absolute difference of the measured rapidity of the spectra from the central rapidity $y_{nn}=1.6$. The spectra are scaled down by a factor of 10 successively. The error bars are statistical only, either shown or smaller than the data point.

agreement between the two data sets is very good. Beam rapidity for Au ions at 11.6A GeV/c is 3.2. Since projectile and target are identical, the cross section is symmetric around mid-rapidity, $y_{nn}=1.6$. This symmetry is used to combine spectra of the same Δy together, where Δy is the separation of the measured rapidity y from the central rapidity $\Delta y=|y-y_{nn}|$. This experiment covers a rapidity range up to $\Delta y=1.05$ with the projectile (or target) rapidity corresponding to $\Delta y=1.6$. The curves in the figure show fits to the spectra based on Eq. (1).

To inspect the shapes of the particle spectra in more detail, the measured particle distributions for π^+, π^-, and protons are displayed in Fig. 2 as a function of m_t-m_0 for the central rapidity interval of $0<\Delta y<0.2$, where the proton spectrum has been multiplied by 0.5 for clarity. The proton spectrum is visibly flatter compared with that for the pions, and it tends to bend down at low m_t-m_0. Unlike the proton spectra measured in reactions induced by lighter projectiles at similar incident energy per nucleon, namely p+A [5] and Si+A [1,2], the proton spectrum here cannot be described satisfactorily by a single exponential fit. The spectrum for π^- is also impossible to describe satisfactorily with a single exponential, since it shows a strong rise at low m_t-m_0. The rise at low m_t-m_0 for π^+ is noticeably less. A statistical analysis over all the measured spectra indicates the typical values of $\chi^2/N_{\rm DF}$ ($N_{\rm DF}\gg 1$) for the single exponential fit are 1.9 for π^+, and 3.6 for π^-. The rise of both pion spectra at low m_t-m_0 might be explained, in part, by the decay of resonances such as Δ isobars which tend to produce relatively

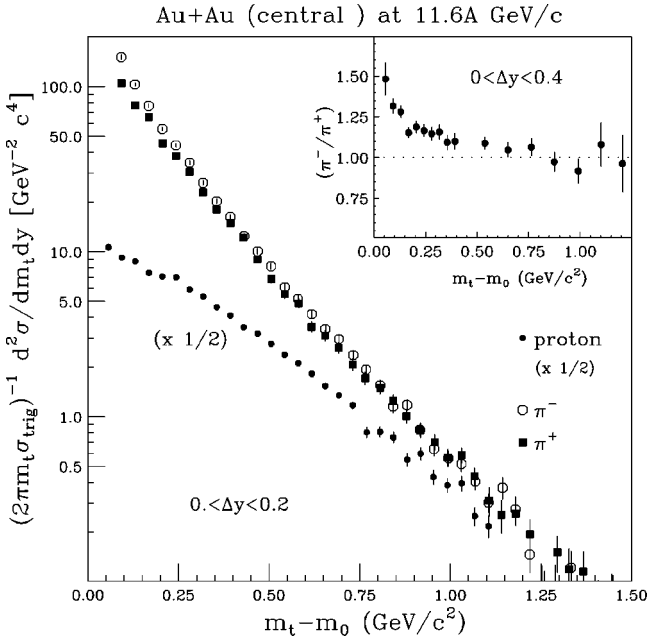

FIG. 2. Measured invariant cross section divided by the trigger cross section for identified pions and protons in the rapidity interval $0<\Delta y<0.2$ as a function of transverse kinetic energy m_t-m_0 (see text). The data for protons, plotted as solid points, is scaled down by a factor of 2. The open circles in the figure are the data for π^-, and the solid squares are that for π^+. The inset shows the ratio of π^-/π^+ as a function of m_t-m_0 for a larger rapidity interval, $0<\Delta y<0.4$. The error bars are statistical only, either shown or smaller than the data point.

low momentum pions [6], but this does not explain the difference in shape. The yield of low momentum pions produced through Δ's prefers π^- [7] because there are more neutrons than protons in the projectile/target. However, the spectra for π^- increase faster than those for π^+ in this region, and there are several possible reasons for this. Among these is the weak decay of the lambda which produces relatively low momentum π^-, and some of these π^- survive the target position cut and show up in the low m_t region. A Monte Carlo calculation based on cascade code, RQMD [8], events and a Geant simulation for the spectrometer indicates that in the region $(m_t$-$m_0)<0.4$ GeV less than 1.5% of the π^- yield is created this way. A major contribution to the differences between the π^- and π^+ spectrum shape may well be their Coulomb interaction with the rest of the comoving media [9–11] which on average is positively charged. In the inset, the ratio (π^-/π^+) is plotted for a larger rapidity bin, $0<\Delta y<0.4$, and the normalization is absolute. At high m_t-m_0, perhaps surprisingly, the ratio approaches one although there are more neutrons than protons in the initial state. Improved statistics in this region could provide an important constraint on dynamic models of the Coulomb modification of pion spectra. The flatter proton spectra are consistent with some degree of outward radial flow [12,13] in the reaction region: qualitatively speaking, particles of larger mass gain more transverse momentum under the influence of the collective flow. Preliminary analysis of deuteron data taken at the same time agrees with this picture [15].

Since it is not a satisfactory parametrization to describe the spectra by a single exponential, a double exponential description is used in order to calculate the rapidity distribution of the particle yield:

$$\frac{d^2\sigma}{2\pi m_t \sigma_{trig} dm_t dy} = A_1 e^{-(m_t-m_0)/B_1} + A_2 e^{-(m_t-m_0)/B_2}. \tag{1}$$

For pions, because there is a rise in the low m_t-m_0 regions, the coefficients of the two exponentials are of the same sign, and only differ in value. This is not the case for protons, however, and two coefficients of different signs are needed to reproduce the turning-down at low m_t-m_0. Thus the inverse slope parameter, as is traditionally used to compare spectra at different rapidities, is less instructive here; instead, the mean transverse momentum [calculated from Eq. (1)] will be used below to serve this purpose. In order to reduce the possible systematic errors in fitting the spectra due to the different coverage in m_t-m_0, each rapidity interval spectra at symmetric rapidities are first combined giving maximum possible coverage in m_t-m_0. As a test of the systematics of the analysis, a comparison is made for cross sections, σ, of overlapped data pairs with the same $(m_t,\Delta y)$, but from rapidities one larger and the other smaller than y_{nn}, by constructing the sum

$$\sum_i \frac{(\sigma_1-\sigma_2)_i^2}{\delta\sigma_i^2},$$

where $\delta\sigma_i^2=(\delta\sigma_1^2+\delta\sigma_2^2)_i$ and the index i runs through all the overlapped pairs. This sum is 169 for π^- with 118 pairs of points and 196 for π^+ with 116 pairs, indicating the difference is larger than the expected statistical fluctuation. To make an estimate of the systematic error for pions, note that if the error on each point is reassigned as $20-30\%$ larger than the statistical fluctuation, the two data sets will appear to be consistent. The similar sum for protons is 64 for 61 pairs of points indicating statistical consistency.

By integrating the parametrization [Eq. (1)] of the spectra over m_t-m_0 in each rapidity bin, one obtains the distribution of particle yield over rapidity, dn/dy. (Other parametrizations yielded similar results to within a few percent.) The upper and middle panels of Fig. 3 show the dn/dy distribution for pions, and protons. Unlike the mean p_t distribution, which only depends on the shape of the m_t-m_0 spectra, dn/dy is proportionally dependent on the absolute normalization of the spectra. We estimate that this overall systematic error in the normalization is about $\pm(10$–$15)\%$. However, the error bars shown in the figure are statistical only and do not reflect the normalization error. It is clear that the protons ''pile up'' at mid-rapidity, confirming the expectation of a large amount of stopping and the concomitant expectation of high baryon density in central Au nuclei collisions. A similar result has been reported for protons in the central rapidity region for Pb+Pb collisions at 158 GeV per nucleon [16]. For a naive comparison, the dotted line in the middle panel is the proton rapidity distribution from central Si+Al at 14.6*A* GeV/*c* [2], multiplied by the mass ratio of the two reactions $197/27=7.3$. This reaction has a maximum around $\Delta y=0.8$, and a minimum around $\Delta y=0$ indicating that there is less stopping and more transparency in Si+Al

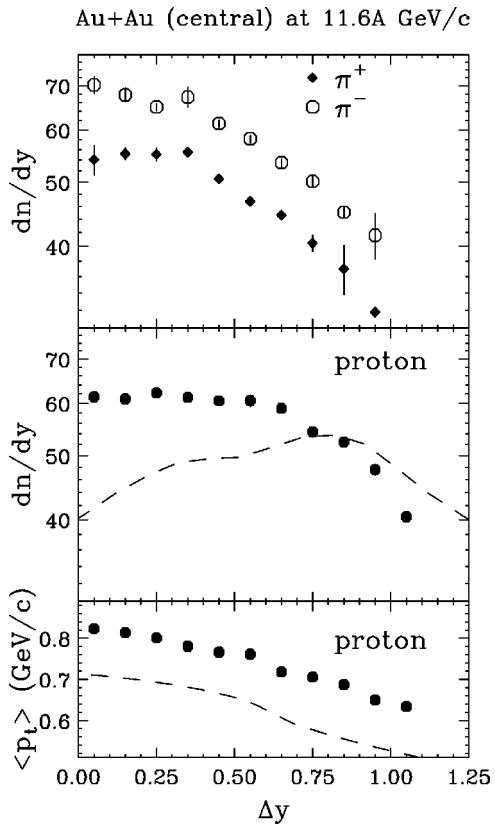

FIG. 3. Rapidity distribution of dn/dy (upper and middle panels) and mean transverse momentum (lower panel) for pions and protons in central Au+Au reactions, where Δy is the absolute difference of the measured rapidity of the spectra from the central rapidity $y_{nn}=1.6$. The open circles in the figure are for π^-, and the solid squares for π^+. Protons are plotted with solid round points. For comparison, the dotted lines are for protons in central Si+Al reactions at 14.6A GeV/c. (The dn/dy for Si+Al is scaled by a factor of 197/27=7.3, the mass ratio of the two reactions.) The error bars are statistical only, either shown or smaller than the data point.

than in Au+Au collisions. Correspondingly, the resulting baryon density implied in central Au+Au is higher. Model calculations based on A Relativistic Cascade (ARC) [14] predict the Au+Au rapidity distribution for protons remarkably well, although it does not get the flattening of the differential transverse momentum spectra. The pion rapidity distribution is also predicted well, but the transverse momentum shapes, in particular the π^-, are noticeably different. These calculations suggest a baryon density of more than about eight times normal nuclear density has been achieved during the evolution of the dynamical process. Both π^+ and π^- basically have the same shape in rapidity, with yields for π^- about 25% higher than that for π^+. As can be seen in the figure, the distribution of pions is narrower in rapidity than that of the protons. In the measured rapidity interval $0.6<y<2.6$, the sum over these distributions gives integrated yields of the produced particles: $N_p=116.0\pm0.5$, $N_{\pi^-}=116.1\pm1.0$, $N_{\pi^+}=94.3\pm1.0$, where the errors are statistical only. The ratio of $(N_{\pi^-}+N_{\pi^+})/N_p$ is about 1.81 ± 0.02.

The lower panel of Fig. 3 shows the mean transverse momentum, $\langle p_t\rangle$, as a function of rapidity for protons. The mean transverse momentum for protons has a maximum at mid-rapidity, and falls gradually toward the target (or projectile) rapidity. Again, for comparison, the dotted line in the figure is data for protons from central Si+Al at 14.6A GeV/c [2] (no factor is multiplied here). These latter values are lower than those of Au+Au, and may indicate fewer multiple collisions between the interacting mesons and baryons have occurred and that a lower effective ''temperature'' has been achieved.

In summary, spectra are measured for the identified hadrons in central Au+Au reactions at 11.6A GeV/c. Unlike the Si+Al results, the rapidity distribution for protons has a maximum around midrapidity, indicating a large degree of stopping and hence strong evidence for high baryon density. Model calculations indicate that the density is increased by about a factor of about 8, and that the lifetime of the high density region is correspondingly longer. It is also found that the proton transverse mass spectra are considerably flatter in central rapidities and at low m_t than in other reactions using lighter ions. This nonexponential shape and large mean p_t for protons may be evidence for collective flow but further analysis of the deuteron and triton spectra is needed to confirm this conclusion. The much more pronounced rise in the π^- spectra than in π^+ at low m_t suggests the presence of a large final-state Coulomb interaction.

This work was supported by the U.S. Department of Energy under contracts with BNL (DE-AC02-76CH00016), Columbia University (DE-FG02-86-ER40281), LLNL (W-7405-ENG-48), MIT (DE-AC02-76ER03069), UC Riverside (DE-FG03-86ER40271), and by NASA (NGR-05-003-513), under contract with the University of California, and by Ministry of Education and KOSEF (951-0202-032-2) in Korea, and by the Ministry of Education, Science, and Culture of Japan.

[1] E-802 Collaboration, T. Abbott *et al.*, Phys. Rev. Lett. **64**, 847 (1990).
[2] E-802 Collaboration, T. Abbott *et al.*, Phys. Rev. C **50**, 1024 (1994).
[3] E-802 Collaboration, T. Abbott *et al.*, Phys. Lett. B **197**, 285 (1987).
[4] E-802 Collaboration, T. Abbott *et al.*, Nucl. Instrum. Methods Phys. Res. A **290**, 41 (1990).
[5] E-802 Collaboration, T. Abbott *et al.*, Phys. Rev. D **45**, 3906 (1992).
[6] R. Brockmann *et al.*, Phys. Rev. Lett. **53**, 2012 (1984).
[7] R. Stock, Phys. Rep. **135**, 259 (1986).
[8] H. Sorge *et al.*, Ann. Phys. (N.Y.) **192**, 266 (1989).
[9] J. P. Sullivan *et al.*, Phys. Rev. C **25**, 1499 (1981).
[10] H. Böggild *et al.*, Phys. Lett. B **372**, 339 (1996).
[11] M. Gyulassy and S. K. Kauffmann, Nucl. Phys. **A362**, 503 (1981).
[12] P. J. Siemens and J. O. Rasmussen, Phys. Rev. Lett. **42**, 880 (1979).
[13] R. Mattiello *et al.*, Phys. Rev. Lett. **74**, 2180 (1994).

[14] S. Kahana *et al.*, in Proceedings of HIPAGS '93, edited by G. Stephans, S. Steadman, and W. Kehoe, p. 263, Report MITLNS-2158.

[15] Z. Chen *et al.*, in Proceedings of HIPAGS '96, edited by C. A. Pruneau *et al.*, Wayne State University, p. 5, Report WSU-NP-96-16.

[16] S. V. Afanasiev *et al.*, Nucl. Phys. **A610**, 188c (1996).